24 th EUROPEAN ROTORCRAFT FORUM
Marseilles, France - 15th-17th September 1998

Calculation of the Flow around Isolated Rotors in Hover and Forward Flight by a Potential and an Euler Method

Référence : AE06

Th . Schwarz

DLR, Institute of Design Aerodynamics

Lilienthalplatz 7, 38108 Braunschweig, Germany

Abstract

Two different methods to calculate the inviscid flow around an isolated rotor-blade are compared: The code HELIFP is based on the full potential equation. It was developed within the BRITE-EURAM project HELISHAPE. The DLR program ROTCATS solves the Euler-equations. Both codes are used to compute the flow around the 7AD rotor designed by Eurocopter France and the BERP rotor developed by GKN-Westland-Helicopters Ltd. within the British Experimental Rotor Program. For each rotor a hover and a forward flight test case are investigated. The grid is generated with the program VIS12.grid, which was also developed within the framework of the HELISHAPE project. For the 7AD rotor the pressure distributions and normal forces computed with both codes are in good agreement. Compared to experimental data some larger discrepancies occur which are due to blade elasticity and wind tunnel interferences. For the BERP rotor the computed pressure distributions are in good agreement, even at the highly swept blade tip. This paper gives also a comparison of the computational performance and the robustness of the codes.

1. Introduction

The flowfield about the rotor of a helicopter is highly complex. There are transonic regions at the blade tip of the advancing blade and regions with separated flow at the retreating blade. Also, vortical wakes are generated at the blade tips. The vortices can induce high velocities on the following rotorblades. These phenomena affect the performance, stability, blade loads, vibrations and the acoustics of the helicopter. For the optimization of a helicopter rotor an accurate prediction of the flowfield is therefore important.

Since wind tunnel tests are to expensive for parameter studies, CFD-Methods can be used instead. The complexity of the problem, however, prevents the computation of the viscous flow around a complete helicopter configuration by solving the Navier-Stokes equations in an industrial context. Therefore, simplified flow models can be applied: By the assumption of an inviscid flow, the Navier-Stokes equations give the Euler-equations. A further simplification can be achieved by assuming an isentropic, irrotational flow. This gives the full potential equation. Another approach to simplify the flow computation is to calculate the flow only around isolated parts of the helicopter instead of the complete configuration.

This paper focuses on the comparison of a full potential method and an Euler method applied to flow computations around a single, isolated rotorblade. To account for the downwash and the wake effects of the whole rotor, a wake model is used

This report presents the results of the author's master thesis in 1997. The work was carried out at the Technical University of Braunschweig, Germany, in co-operation with the Institute of Design Aerodynamics of DLR and GKN-Westland Helicopters Ltd., Great Britain.

2. Governing Equations

By the assumption of an inviscid flow the Navier-Stokes-equations yield the Euler-equations. They are a system of five coupled, nonlinear differential equations of first order in time:

$$\frac{\partial}{\partial t}\vec{U} + \vec{\nabla}\bar{F} = 0 \qquad (1)$$

with the vector of the conservative variables $\vec{U}$ and the flux density tensor $\bar{F}$:

$$\vec{U} = \begin{bmatrix} \rho \\ \rho\vec{q} \\ \rho E \end{bmatrix} \quad ; \quad \bar{F} = \begin{bmatrix} \rho\vec{q} \\ \rho\vec{q} \otimes \vec{q} + p\bar{I} \\ \rho\vec{q}H \end{bmatrix} \qquad (2)$$

Where ρ denotes the density, $\vec{q}$ the vector of velocities p the pressure and $\bar{I}$ the identity matrix. The total specific enthalpy H can be calculated from the total specific energy E by:

$$H = E + \frac{p}{\rho} \qquad (3)$$

The system of equations is closed by:

$$p = (\gamma - 1)\rho\left(E - \frac{\vec{q}^2}{2}\right) \tag{4}$$

A further simplification of the flow equations is obtained with the approximation of an inviscid, irrotational and isentropic flow. In this case, the complete flowfield can be described by a single scalar variable, the so called potential Φ. From the known potential, the velocity components can be determined by:

$$\vec{q} = \vec{\nabla}\Phi \tag{5}$$

The Euler equations simplify to a single differential equation of first order in time:

$$\frac{\partial \rho}{\partial t} + \vec{\nabla} \cdot (\rho \vec{\nabla}\Phi) = 0 \tag{6}$$

The correlation between the density and the potential is given by the Bernoulli-equation:

$$\left(\frac{\rho}{\rho_\infty}\right)^{\gamma-1} = \frac{a^2}{a_\infty^2} = 1 - \frac{\gamma - 1}{a_\infty^2}\left(\frac{\partial \Phi}{\partial t} + \frac{\vec{q}^2}{2}\right) \tag{7}$$

where a is the speed of sound, γ is the isentropic coefficient and the index ∞ denotes the freestream state.

The drawback of the simplifications introduced in the full potential flow model is that flow phenomena like strong shocks and vortices are not correctly simulated.

3. Numerical Methods

3.1 Potential Method ‚HELIFP' developed within BRITE-EURAM project HELISHAPE

For the numerical method HELIFP [1] the full potential equation (5) and the Bernoulli-equation (6) are transformed from the Galilean frame of reference to a body conforming frame linked to the moving rotor blade. This transformation gives the full potential equation of the form

$$\frac{\partial}{\partial t}\left(\frac{\rho}{J}\right) + \vec{\nabla}^C \cdot \left(\frac{\rho \vec{Q}}{J}\right) = 0 \tag{8}$$

and the Bernoulli Equation

$$\frac{a^2}{a_\infty^2} = 1 - \frac{\gamma - 1}{a_\infty^2}\left(\frac{\partial \Phi}{\partial t} + \frac{1}{2}\left(\left(\vec{Q} + H\frac{\partial \vec{r}_r}{\partial t}\right) \cdot \vec{\nabla}^C \Phi\right)\right) \tag{9}$$

where

$$\vec{Q} = H\frac{\partial \vec{r}_r}{\partial t} + HH^T\vec{\nabla}^C\Phi \tag{10}$$

In equations (7),(8),(9) the matrix H is the Jacobian matrix of the transformation from the Galilean frame to the computational frame and J is the determinant of H. Furthermore, $\vec{\nabla}^C$ is the gradient operator in the computational frame. $(\partial \vec{r}_r)/(\partial t)$ is the velocity of the cartesian coordinates of a frame linked with the blade relative to the Galilean frame of reference.

The full potential equation is spatially discretizied according to the method of Jameson and Caughey [2]. To prevent high frequency oscillations of the flow quantities (known as odd-even decoupling), additional lumping terms are introduced in the discretizied potential equation [3].

The potential equation allows for expansion shocks, which are non-physical solutions. To provide the necessary artificial viscosity needed to suppress expansion shocks and to stabilize the computation in supersonic regions, a streamwise density-flux-biasing is applied.

The basic assumptions made in the potential model are that the flow is inviscid, irrotational and isentropic. This yields an incorrect calculation of the strength and position of shocks in transonic flow. For the first approximation, that the entropy production only occurs across the shock waves, the error can be reduced with an entropy correction.

In order to recover the freestream correctly, a free stream flux correction is introduced into the discrete potential equation.

For the temporal discretization an implicit formulation is used. In order to obtain an equation for the velocity potential increment, a first order time linearization is applied to the density and flux terms. The resulting system of equations is solved by approximate factorisation. For each time step, the solution can be improved by a newton iterative technique.

To solve the full potential equation, a set of boundary conditions has to be imposed. At the body, the flow is tangential to the surface. If inflow due to wake induced velocities or elastic blade motion is modelled, the tangential condition is modified by adding a transpiration velocity. The flow normal to the wake is continuous. At the inboard boundary two-dimensional perturbation flow is applied. Riemann invariants are used at the far field boundary.

The Program HELIFP can be applied for a single wing or rotorblade and a one block grid with CH-topology.

3.2 Numerical Method ‚ROTCATS' developed by DLR

For the DLR method ROTCATS [4][5], the discretiza-

tion of the Euler-equations starts from the integral form of equation (1), which is transformed to a cartesian, blade fixed co-ordinate system:

$$\frac{\partial}{\partial t}\int_{V_r} \vec{U}_r \cdot dV_r + \oint_{\partial V_r} \vec{F}_r \cdot d\vec{S}_r + \int_{V_r} \vec{G}_r \cdot dV_r = 0 \quad (11)$$

In this equation V_r denotes the volume and $\vec{S}_r$ the surface vector of the control volume and

$$\vec{U}_r = \begin{bmatrix} \rho \\ \rho\vec{q}_r \\ \rho E_r \end{bmatrix} \quad ; \quad \vec{F}_r = \begin{bmatrix} \rho(\vec{q}_r - \vec{q}_{b,r}) \\ \rho\vec{q}_r \otimes (\vec{q}_r - \vec{q}_{b,r}) + p\vec{I} \\ \rho(H_r\vec{q}_r - E_r\vec{q}_{b,r}) \end{bmatrix}$$

$$\vec{G}_r = \begin{bmatrix} 0 \\ \rho(\vec{q}_r \times \vec{\omega}_r) \\ 0 \end{bmatrix} \quad (12)$$

The velocity vector given in the body fixed frame is split into two parts: The velocity $\vec{q}_{b,r}$ is due to the movement of the co-ordinates of the body fixed frame relatively to the Galilean frame. The vector $\vec{q}_r$ is determined by the projection of the velocity $\vec{q}$ given in the Galilean frame to the axes of the blade fixed frame. Therefore, the absolute values of the velocities given in the Galilean frame and the moving frame are identical. This is especially important for the formulation of the farfield boundary condition.

The transformation into a moving frame of reference introduces an extra source term $\vec{G}_r$, which depends on the angular velocity $\vec{\omega}_r$ of the moving frame relatively to the Galilean frame. The system of equations is closed with

$$p = (\gamma - 1)\rho\left(E_r - \frac{\vec{q}_r^{\,2}}{2}\right) \quad (13)$$

and

$$H_r = E_r + \frac{p}{\rho} \quad (14)$$

The enthalpy and the energy in the moving frame and the Galilean frame are identical.

$$E_r = E \quad ; \quad H_r = H \quad (15)$$

For the DLR method ROTCATS the discretization in space and time is separated following the method of lines (Jameson and al. [6]), using a cell-centered finite volume scheme for the spatial discretization. To avoid oscillations, a blend of first and third order dissipative terms is introduced.

For the integration in time, an explicit five-stage Runge-Kutta time-stepping scheme is used.

The convergence for steady and unsteady computations can be accelerated by implicit residual smoothing. For steady calculations, local time stepping and enthalpy/rothalpy damping can be used, too.

For the boundary condition at the body, the flux through the surface is zero. To simulate wake induced velocities or blade elasticity, a penetration velocity different to zero can be prescribed at the surface. At the far field, characteristic variables are used. No extra treatment is applied at the hub. The far field condition is used there. At the wake, the continuity of the flow is ensured.

The program ROTCATS can be applied for arbitrary, multiblock meshes. The chimera-technique is implemented, too [7].

4. Grid Generator

For the method HELIFP, a special algebraic grid generator VIS12.grid has also been developed within the BRITE-EURAM project HELIFUSE [1]. It generates structured grids with a CH-topology around a single wing or rotor blade. VIS12.grid is easy to use and generates a grid for a given surface geometry in about five minutes on a workstation.

5. Numerical Results - Four-Bladed 7AD Rotor

The fully instrumented 7AD rotor designed by Eurocopter France has been tested at the S1 wind tunnel at the Modane testcenter and at the German-Dutch Wind Tunnel (DNW) [8][9]. The rotor has a SPP8 parabolic anhedral tip with taper and sweep. (see Fig. 1). It has

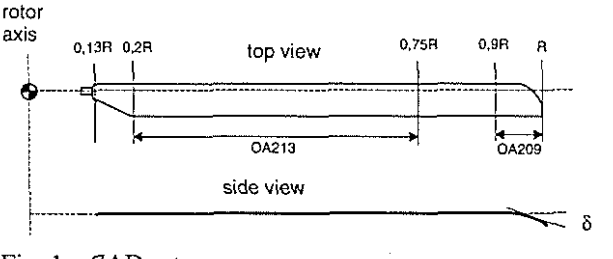

Fig. 1: 7AD rotor

OA213 airfoil sections from the blade root to r/R=0.75 and OA209 airfoil sections from r/R=0.9 to the blade tip. The rotor has a geometric twist corresponding to a linear aerodynamic twist of -3.95°/m and has an aspect ratio of 15. Experimental data for the pressure coefficients are available at five spanwise sections (r/R=0.5, r/R=0.7, r/R=0.825, r/R=0.915, r/R=0.975).

5.1 Grid Generation

Because of two limitations of HELIFP, the grid genera-

tion with VIS12.grid was an iterative process: The hub boundary has to be located at a radial position where the flow on the retreating blade is never reversed. The second demand of HELIFP is that all cell volumes are not smaller than 10^{-8}. This restriction is due to numerical errors at matrix inversion during the computation and makes it difficult to create a fine grid.

The CH-grid for the 7AD rotor is shown in Figure 3. It consists of 160 cells in chordwise direction with 108 cells on the blade surface, 24 cells normal to the blade surface and 34 cells in radial direction with 21 cells on the blade surface. All presented flow calculations for the 7AD rotor are computed with this grid.

5.2 7AD Rotor in Hover

The first test case is the 7AD rotor in hover with a tip Mach number of $M_{\omega R} = 0.617$. The pitching angle Θ and the flap angle β are independent of the azimuth angle Ψ:

$$\Theta(\Psi) = 7.47°$$

$$\beta(\Psi) = 0°$$

The downwash velocities for this test case have been computed with the prescribed wake downwash model of Beddoes ([10][11]).

To check the convergence of the computation, a reduction of the residual by five orders of magnitude has been demanded for ROTCATS. With HELIFP only a reduction of three orders of magnitude was achieved.

A comparison of the computed pressure distributions (Fig. 4) shows a good agreement for the tip region. Some larger discrepancies occur at r/R = 0.50, where HELIFP predicts a higher lift than ROTCATS. This can be explained by the different boundary condition applied at the hub.

The numerical results are in good agreement with the experimental data.

It must be noted, that the prediction of the downwash velocities with a prescribed wake model for a rotor in hover still has a lot of uncertainties and gives not always satisfactory results.

5.3 7AD Rotor in Forward Flight

For this instationary test case, the tip Mach number is $M_{\omega R} = 0.617$ and the free stream Mach number is $M_\infty = 0.258$. This corresponds to an advance ratio of $\mu = 0.419$. The pitching and flapping motions are given by:

$$\Theta(\Psi) = 11.36° + 1.9181° \cos(\Psi) - 5.0778° \sin(\Psi)$$

$$\beta(\Psi) = 2.203° - 5.0778° \cos(\Psi)$$

The rotor shaft angle is -11.8° (rotor plane tilted in the onflow direction).

The downwash velocities have been kindly made available by GKN Westland Helicopter Ltd. .

To check the periodicity of the flow it has been demanded, that the the normal forces calculated during two consecutive revolutions of the rotor do not differ by more than one percent. The convergence in time is ensured, since halving the time step does not change the normal forces computed for one revolution of the rotor by more than one percent. The same criterion has been used to determine the required number of newton iterations for HELIFP.

The computed nondimensional pressure distributions for the 7AD rotor in forward flight are shown in Figure 5 to Figure 7 for the radial stations r/R=0.50, r/R=0.825 and r/R=0.975. A comparison of the numerical results shows a good agreement in the tip region. As for the hover test case, some larger discrepancies occur at r/R = 0.50, which can be explained by the different boundary condition applied at the hub.

Near the tip section of the advancing blade transonic flow with shocks appears. The shock intensity calculated with HELIFP without entropy correction is stronger than predicted by ROTCATS and the shock wave location is slightly downstream compared to the solution of the Euler equations. This results from the assumption of an isentropic flow for the potential flow model.

The shock position is not improved if the entropy correction is considered, but the shock is slightly weaker. Also, the entropy correction only influences the pressure downstream the shock, whereas the pressure distribution upstream the shock and on the lower surface do not change. (Remark: Later versions of HELIFP than used for this work have an improved algorithm for the entropy correction, which gives a better prediction of the shock location and the shock strength).

Some differences at the blade tip may be due to the irrotational flow assumption for the potential flow, which do possibly not give the correct production of vorticity.

A comparison with experimental data shows good agreement at r/R=0.825 and r/R=0.975. The discrepancies in the pressure distributions at r/R=0.50, Ψ=0° and Ψ=180° can be explained with the disturbance of the flow by the rotor support but also separated flow caused by the rotor shaft. For the retreating blade at r/R=0.50 and Ψ=270° the flow may be separated. Deviations at the blade tip may be due to the elastic deformations of the rotor blade during the experiment [8][12]. Another reason might be inaccurate downwash velocities

In Figure 8 the nondimensional normal force

$$c_n \cdot M^2 = \frac{N}{\frac{\rho_\infty}{2} a_\infty^2 \cdot l \cdot l_E}$$

is plotted versus the azimuth (N = normal force, ρ_∞ = free stream density, a_∞ = free stream speed of sound, l = chord length, l_E = unit length). In general, the computations with HELIFP give a larger normal force than calculated with ROTCATS. Possible reasons for the deviations at the blade root and tip were already discussed for the pressure distributions.

It can also be observed that inexplicable oscillations occur in the $c_n \cdot M^2$-plots calculated with HELIFP using the entropy-correction in transonic flow.

For the nondimensional normal forces, the agreement with experimental data is fair. In general, ROTCATS gives better results than HELIFP. Reasons for discrepancies were already discussed for the pressure distributions. It can be noted that the same deviations between experiment and computations have been observed in [13].

6. Numerical Results - Four-Bladed BERP Rotor

The four-bladed BERP rotor has been developed by GKN-Westland Helicopters Ltd. within the British Experimental Rotor Program. With a blade of this technology, a new world speed record for helicopters was set in 1986. The unusual planform of the blade is shown in Figure 2. To reduce transonic effects, the last 15% of

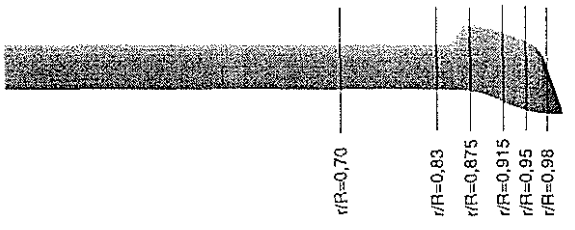

Fig. 2: BERP rotorblade

the span are swept back. Since a simple swept tip shifts the aerodynamic center behind the feathering axis, which leads to control problems, leading edge area was added at the tip forming the characteristic notch at r/R=0.85. The delta-wing like planform at the extreme spanwise location improves the performance of the blade at a high angle of attack by producing a stable vortex structure over the wing surface. This feature in combination with high performance RAE airfoils lead to the impressive performance of the BERP blade. A detailed description of the blade and the design ideas can be found in [14].

The geometry data of the BERP blade and the airfoil co-ordinates are not publicly available. Instead, NACA 00XX profiles are used with a thickness of 12% from the blade root at r/R=0.2 to r/R=0.63, 11% from r/R=0.66 to r/R=0.84 and 8% thickness from r/R=0.86 to the tip.The blade planform is chosen according to [18]. The blade has a linear twist of -6.0° from r/R=0.0 to r/R=1.0. The anhedral of the original BERP blade is not considered because of its unknown geometry.The aspect ratio of the blade is 16.21.

The hover performance of the BERP blade has been studied with inviscous and viscous methods [15][16][17][18]. Numerical analyses for the BERP rotor in forward flight are not know to the author. Experimental pressure data are not publicly available.

For this paper, a hover and a forward flight test case are studied. The data for the test cases were obtained from flight tests performed with the ‚G-Lynx'. They were kindly provided by GKN-Westland Helicopters Ltd. The wake induced velocities have also been computed by GKN-Westland Helicopters Ltd. .

6.1 Grid Generation

The grid generation was difficult: Because of the very small chord length at the blade tip, the mesh cells become extremely small there. This contradicts with the demand of HELIFP that the volumes of the grid cells are not smaller than 10^{-8}. Therefore an iterative procedure was necessary to create a sufficient fine grid. The final grid presented in Figure 9 consists of 160x49x24 cells with 108x34 cells on the blade surface.

6.2 BERP Rotor in Hover

For this test case, the tip Mach number is $M_{\omega R} = 0.642$. The blade motion is given by:

$$\Theta(\Psi) = 8{,}4°$$
$$\beta(\Psi) = 0°$$

Figure 10 illustrates the comparison of the pressure distributions computed with HELIFP and ROTCATS. At r/R=0.7 HELIFP computes a higher lift than ROTCATS. For r/R = 0.915 and even at the blade tip, the pressure distributions are nearly identical.

6.3 BERP Rotor in Forward Flight

The freestream mach number for this test case is M_∞=0.17 with a tip mach number of $M_{\omega R}$=0.69 and an advance ratio of μ=0.246. The flapping and pitching motions of the blade are given by:

$$\Theta(\Psi) = 2{,}15° - 3{,}2° \cos(\Psi) + 0{,}3° \sin(\Psi)$$
$$\beta(\Psi) = 0°$$

The shaft angle is 0°.

As for the 7AD rotor, the independency of the numerical results with respect to the time step and the periodicity of the flow is ensured with a convergence study.

Figure 11 to Figure 13 illustrate the comparison between the pressure distributions computed with HELIFP and ROTCATS. The results show a good agreement, even at the highly swept tip. Since no

shocks appear, the pressure distributions calculated with HELIFP with and without entropy correction are identical.

As shown in Figure 14, the nondimensional normal forces calculated with HELIFP are slightly larger than calculated with ROTCATS, but the overall agreement is good.

7. Computational Performance

The calculations have been performed on a NEC-SX4. This is a vector computer with four processors and a peak performance of 1400 MFLOPS (million floating point operations per second) per processor.

Since it is not possible to do parallel computations with HELIFP and ROTCATS, all calculations were carried out on a single processor. The following tables present the CPU time consumption of HELIFP and ROTCATS to compute the converged solution in hover and one rotor revolution in forward flight:

HELIFP (Full Potential Equation)		
test case	number of time steps	CPU time consumption*
7AD, hover	600	244 / 264 s (ca. 4 min)
7AD, forward flight	2880	3500 / 3850 s (ca. 1 h)
BERP, hover	600	310 / 340 s (ca. 5 min)
BERP, forward flight	1440	2620 / 2830 s (ca. 45 min)

* (CPU-time without/with entropy correction)

ROTCATS (Euler-Equations)		
test case	number of time steps	CPU time consumption
7AD, hover	1000	638 s (ca. 11 min)
7AD, forward flight	18000	11610 s (ca. 3 h 15 min
BERP, hover	700	633 s (ca. 11min)
BERP, forward flight	36000	33744 s (ca. 9h 20 min)

The comparison of the CPU time shows that HELIFP requires less CPU time for the flow calculation for one period than ROTCATS. This is partly due to the more complex system of Euler equations compared to the full potential equation. But the main reason is the explicit time stepping scheme of ROTCATS: the maximum allowed time step required to ensure stability is given by the Courant-Friedrich-Levi condition for the smallest grid cell. This requires very small time steps especially for the BERP blade. For the implicit time stepping scheme used in HELIFP, the only restriction for the maximum time step is that all flow phenomena have to be represented accurately.

It has to be considered that the periodicity of the flow is reached with ROTCATS after a quarter revolution of the rotor, whereas a computation with HELIFP requires at least a half period.

8. Conclusion

Two methods for the calculation of the flowfield about an isolated rotor blade are compared. The method ROTCATS by DLR solves the system of Euler equations whereas the method HELIFP developed within the BRITE-EURAM project HELISHAPE is based on the full potential equation. Both methods are applied to the 7AD rotor and the BERP rotor. For each rotor, a hover and a forward flight test case are investigated.

The generation of the grids with the VIS12.grid grid-generator has been an iterative process, because HELIFP requires that the smallest cell volume is not below 10^{-8}. This delayed especially the generation of a grid for the BERP blade, since the grid has extremely small cells at the blade tip.

A comparison of the computed pressure distributions and $c_n M^2$ plots show good agreement. Some discrepancies occur at the inner blade sections, where HELIFP predicts a higher lift than ROTCATS.

Additional differences in the calculations occur in transonic flow. The two methods give different shock strengths and shock positions. The results of HELIFP are not improved by an entropy correction, but the $c_n \cdot M^2$-values oscillate in transonic flow when calculated with HELIFP and entropy correction. (Later versions of HELIFP than used for this work have an improved algorithm for the entropy-correction which gives better results).

Experimental pressure data for the 7AD rotor are in an fair agreement with the computations. Some discrepancies occur in the calculated and measured normal forces. This may be due to wind tunnel interferences and blade elasticity.

Because of the good results and the small amount of CPU time per calculation, HELIFP can be used for rotorblade flowfield computations. To make the code more robust, the tolerance for small grid cells has to be

improved.

The computations show that ROTCATS is a very robust method: reversed flow at the rotorblade or small grid cells do not cause any problems. Another advantage of the Euler-method is that vortices and shocks are captured without any additional modelling. A disadvantage is the high consumption of CPU time. This could be improved by calculations with an implicit time-stepping scheme.

9. Acknowledgement

The author wishes to express his gratitude to Dr. A. Kokkalis of GKN-Westland Helicopters Ltd. for arranging a short secondment of the author to GKN-Westland Helicopters Ltd.in Great Britain, where some of the presented work was done. Thanks also for his cooperation in providing the wake-files and the instruction on HELIFP.

Thanks to Prof. A. Das, Dr. N. Kroll and Dr. K. Pahlke of DLR for the helpful discussions.

Finally, the author will like to thank all the partners from Task 2 of the BRITE/EURAM - HELIFP project for giving their permission and providing the HELIFP and VIS12.grid codes used in this work.

10. References

[1] M. Costes, J.C. Le Balleur, L. Gasparini, L. Vigevano, M.H.L. Hounjet, A. Kokkalis, J.V. Miller, M.Spruce, A. Pagano, P. Renzoni, A. Rocchetto, F. Toulmay, "Development of a common European Unsteady Full Potential CFD Code for Helicopter Rotors in Hover and Forward Flight", AHS 53rd annual Forum, Virginia Beach, Virginia, USA, April 29 - May 1, 1997

[2] C. Hirsch, "Numerical Computation of Internal and External Flows",Volume 1 & 2, Jhon Wiley&Sons

[3] M.H.L. Hounjet, B.J.G. Eussen, "Outline and Application of the NLR Aeroelastic Simulation Method", ICAS-94-5.8.2, September 1994

[4] N. Kroll,"Berechnung von Strömungsfeldern um Propeller und Rotoren im Schwebeflug durch die Lösung der Euler-Gleichungen", DLR-Forschungsbericht 89-37

[5] K. Pahlke, J. Raddaz, "3D Euler Methods for Multibladed Rotors in Hover and Forward Flight", Nineteenth European Rotorcraft Forum, Paper C20, Cernobbio (Como), Italy, 14. - 16. September, 1993

[6] A. Jameson, W. Smidt, E. Turkel, "Numerical Solutions of the Euler Equations by Finite Volume Methods Using Runge-Kutta Time Stepping Schemes", AIAA-Paper 81-1259 (1981)

[7] K. Pahlke, J. Raddatz, "Flexibility Enhancement of Euler Codes for Rotor Flows by Chimera Techniques", 20th European Rotorcraft Forum, Amsterdam, The Netherlands, 4. - 7. October, 1994

[8] M. Allongue, J. P. Drevet, "New Rotor Test Rig in the Large Modane Wind Tunnel", Fifteenth European Rotorcraft Forum, Paper No. 98, Amsterdam, Netherlands, 12. - 15. September, 1989

[9] K.-J. Schultz, W. Splettstößer, B. Junker,, W. Wagner, "A Parametric Wind Tunnel Test on Rotorcraft Aerodynamics and Aeroacoustics (HELISHAPE) -- Test Procedures and Representative Results", 22nd European Rotorcraft Forum, Brighton, UK, 17. - 19. September, 1996

[10] T.S. Beddoes, "A Wake Modell for High Resolution Airloads", International Conference on Rotorcraft-Basic-Research, Research Triangle Parc, N.C., 1985

[11] Berend v. d. Wall, "Analytische Formulierung der instationaeren Profilbeiwerte und deren Anwendung in der Rotorsimulation", DLR-FB-90-28, Deutsche Forschungsanstalt für Luft und Raumfahrt e.V. 1990

[12] P. Beaumier, M. Costes, R.Gaveriaux, "Comparison between FP3D Full Potential Calculations and S1 Modane Wind Tunnel Test Results on Advanced Fully Instrumented Rotors", Nineteenth European Rotorcraft Forum, Paper C12, Cernobbio (Como), Italy, 14. - 16. September, 1993

[13] J.-C. Boniface, K. Pahlke, "Calculations of Multibladed Rotors in Forward Flight Using 3-D Euler Methods of DLR and ONERA", 22nd European Rotorcraft Forum, Paper No. 58, Brighton, UK, 17. - 19. September, 1996

[14] F.J. Perry, "Aerodynamics of the Helicopter World speed record", 43rd Annual National Forum of the American Helicopter Society, May 1987

[15] Earl P.N. Duque, "A Numerical Analysis of the British Experimental Rotor Program Blade", Fifteenth European Rotorcraft Forum, Paper No. 0, Amsterdam, Netherlands, 12. - 15. Septemper, 1989

[16] B. Wake, T. Egolf, "Application of a Rotary-Wing Viscous Flow Solver on a Masively Parallel Computer", American Institute of Aeronautics and Astronautics, 28th Aerocpace Sciences Meeting, 8. - 11. January, 1990, Reno, Nevada, USA

[17] G.R. Srinivasan, V. Raghaven, E.P.N. Duque, W.J. McCroskey, "Flowfield Analysis of Modern Helicopter Rotors in Hover by Navier-Stokes Method", Journal of the American Helicopter Society,Volume 38-Number 3, July 1993

[18] J. Wild, "Numerische Simulation der dreidimensionalen Umströmung von Blattspitzen an Hubschrauberrotoren im Schwebeflug", Institutsbericht 129-95/4, Institut für Entwurfsaerodynamik, Deutsche Forschungsanstalt für Luft und Raumfahrt e. V.

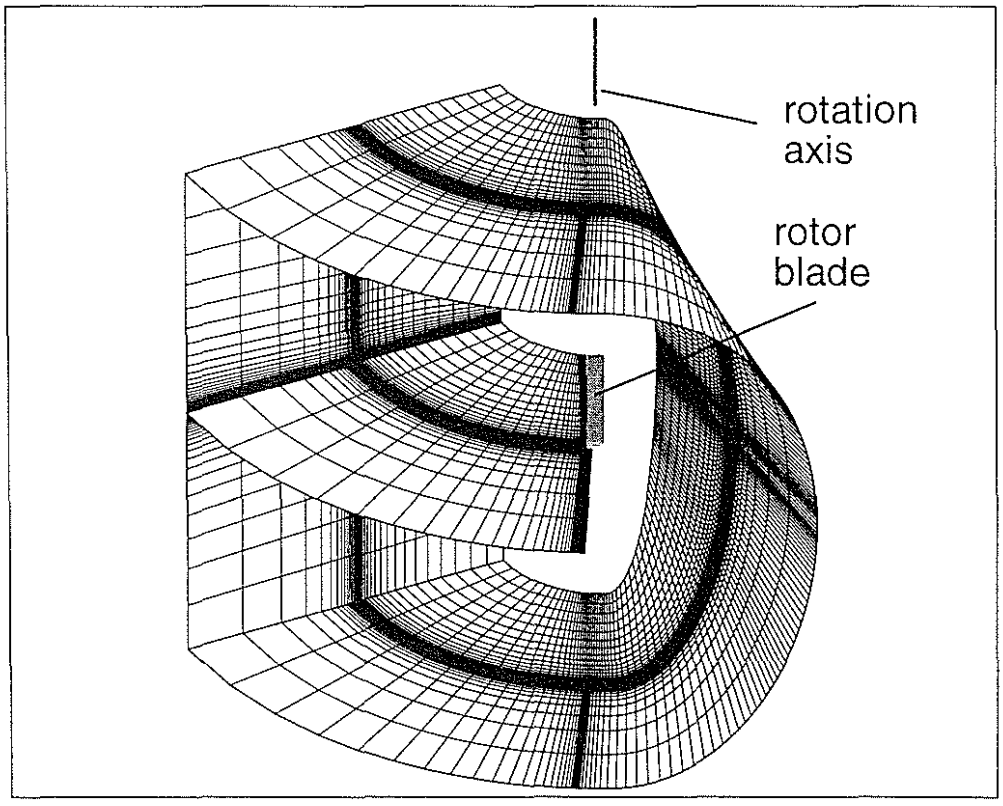

Fig. 3: Grid around 7AD blade

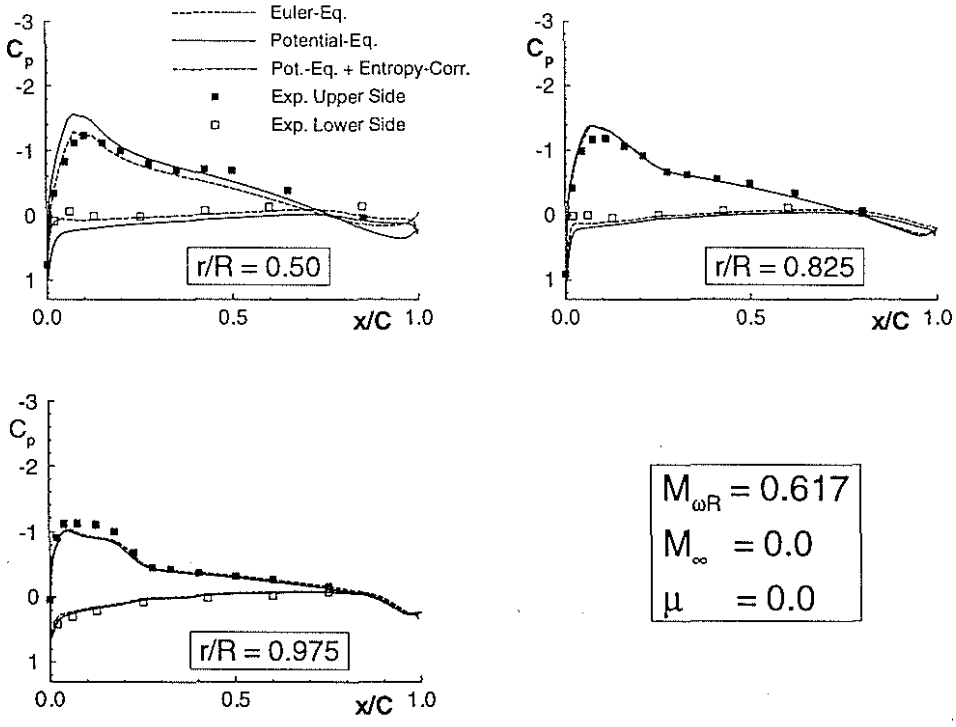

Fig. 4: Pressure distributions for the 7AD rotor in hover

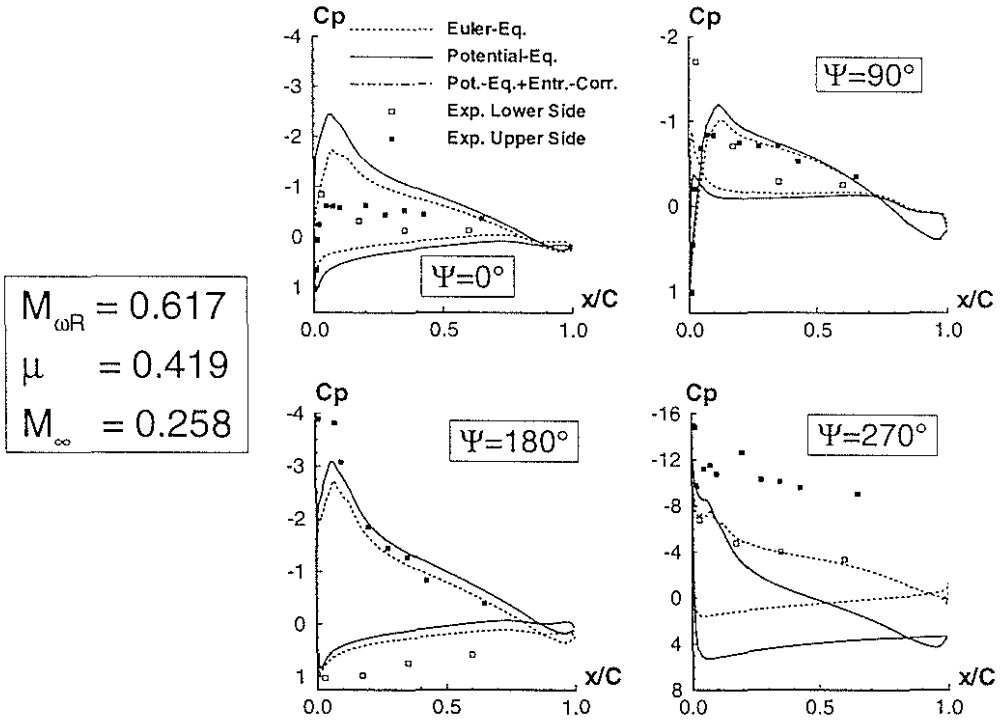

Fig. 5: Pressure distribution at r/R = 0.50 for the 7AD rotor in forward flight

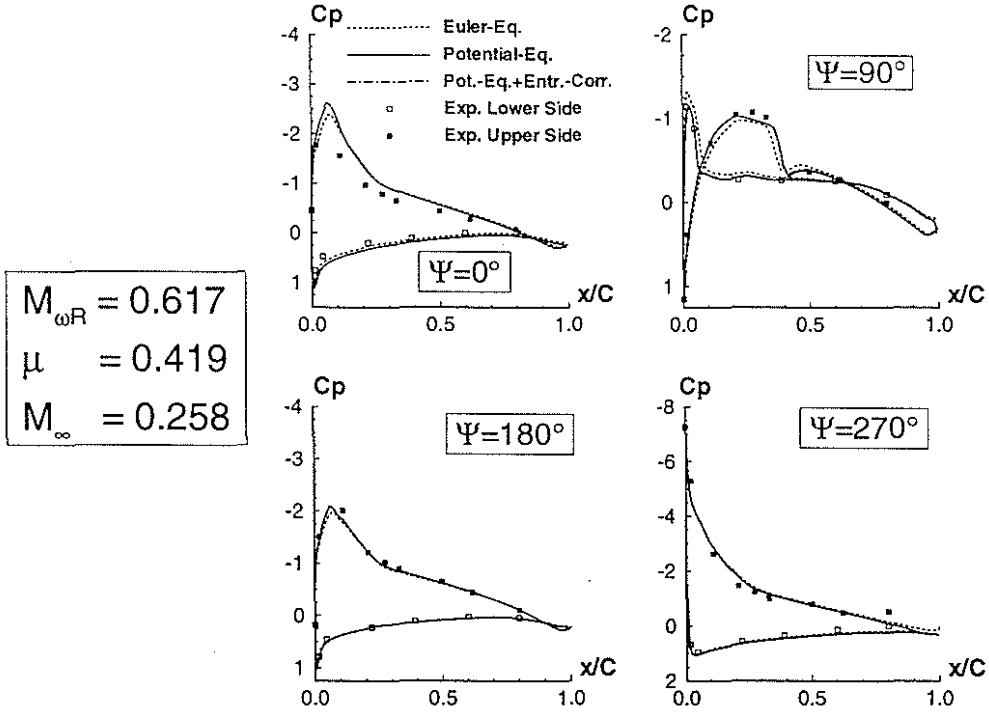

Fig. 6: Pressure distribution at r/R = 0.825 for the 7AD rotor in forward flight

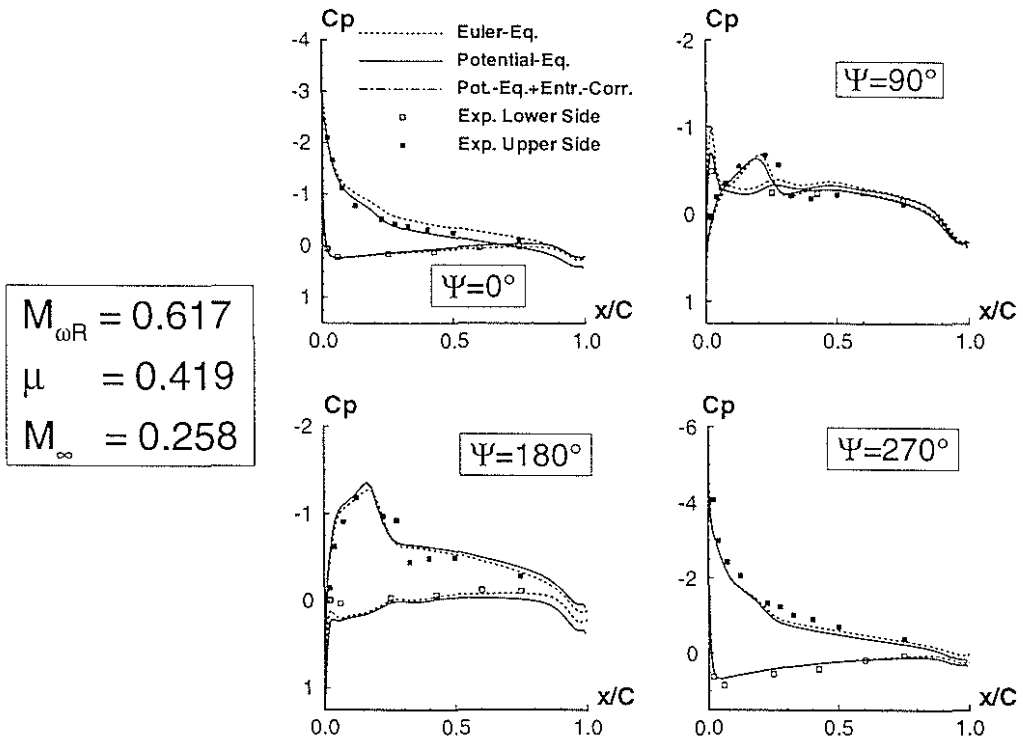

Fig. 7: Pressure distribution at r/R = 0.915 for the 7AD rotor in forward flight

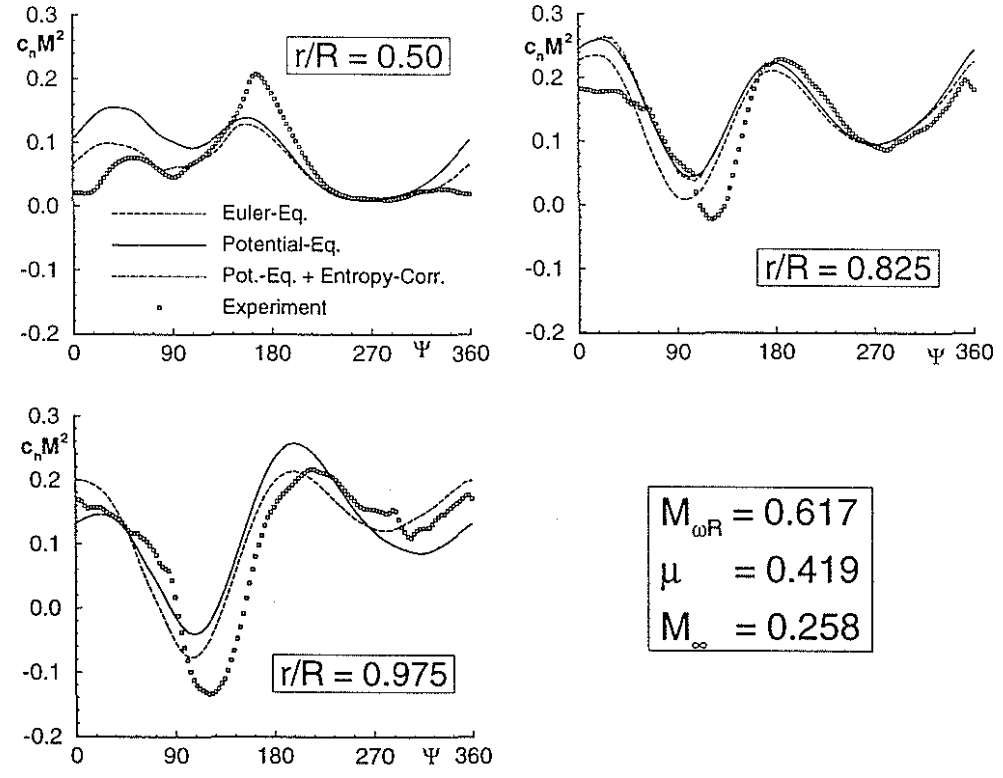

Fig. 8: Nondimensional normal forces for the 7AD rotor in forward flight

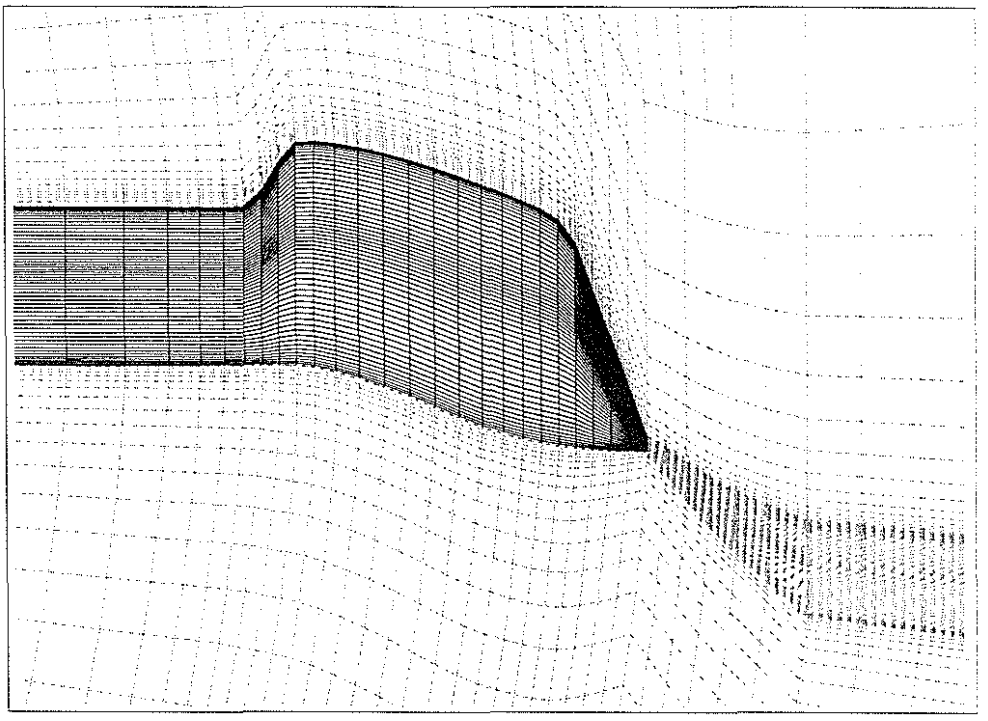

Fig. 9: Grid around BERP blade near the tip region

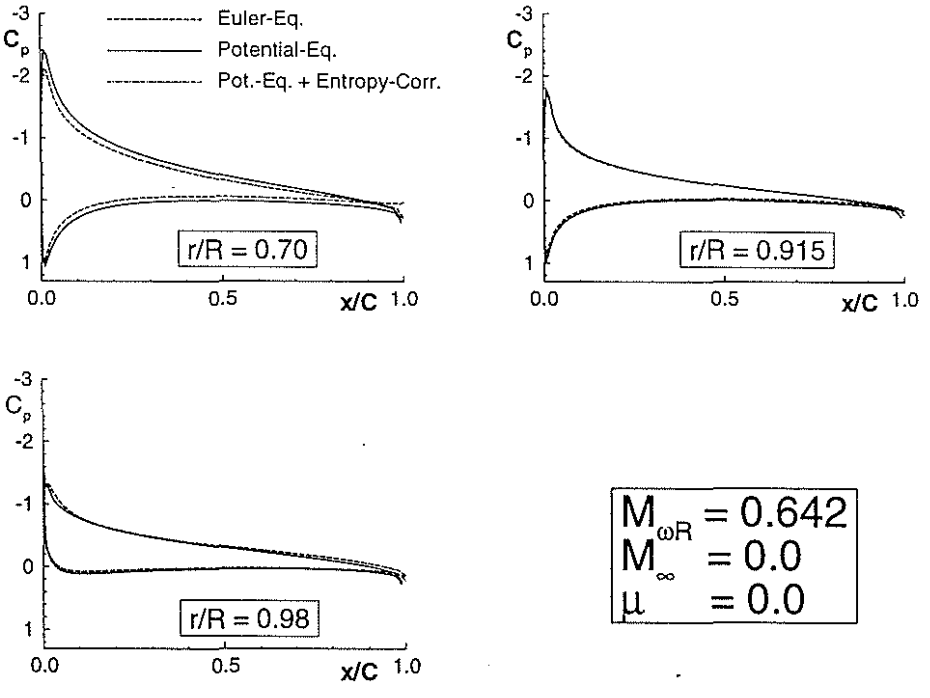

Fig. 10: Pressure distributions for the BERP blade in hover

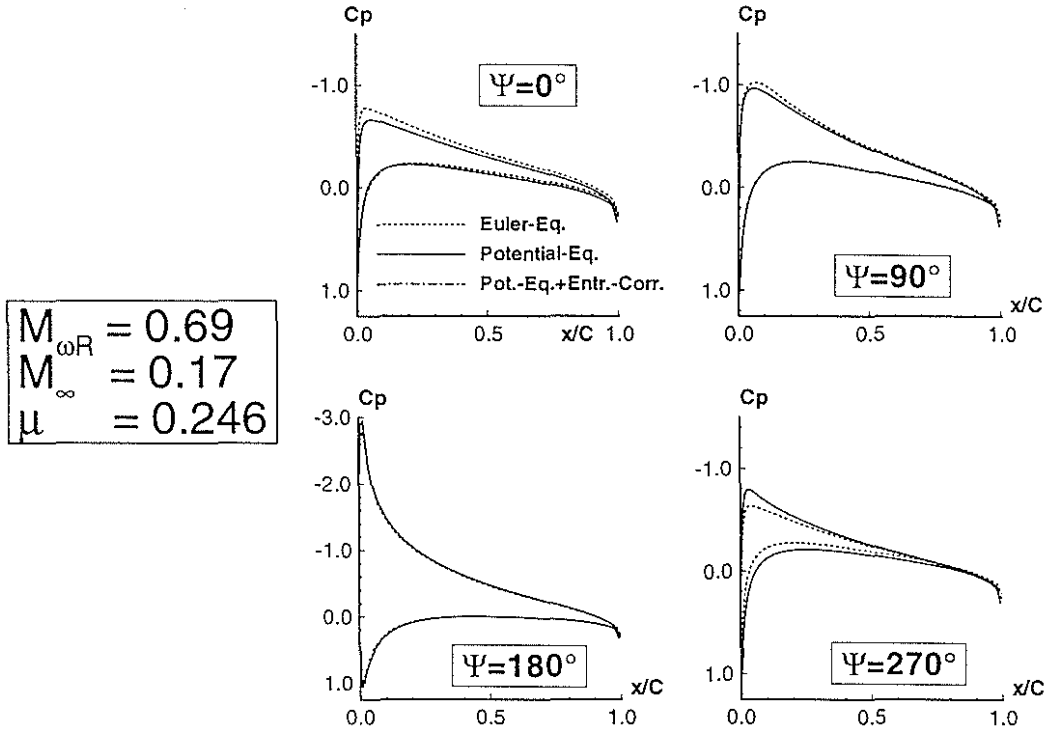

Fig. 11: Computed pressure distributions for the BERP blade in forward flight at r/R = 0.70

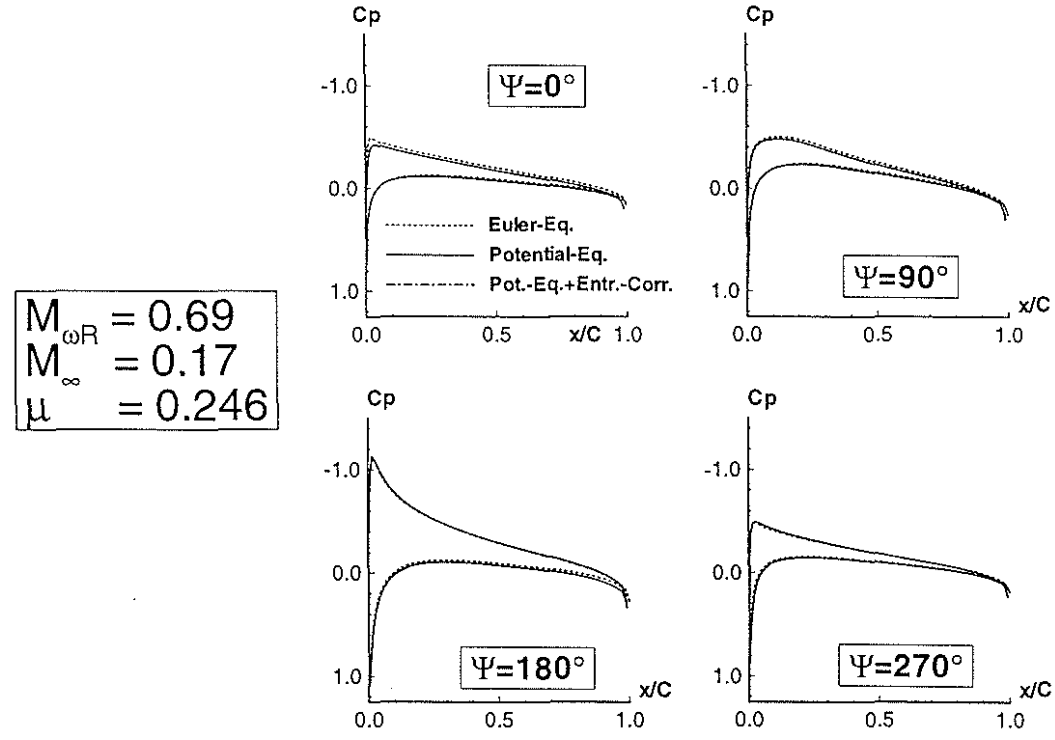

Fig. 12: Computed pressure distributions for the BERP blade in forward flight at r/R = 0.915

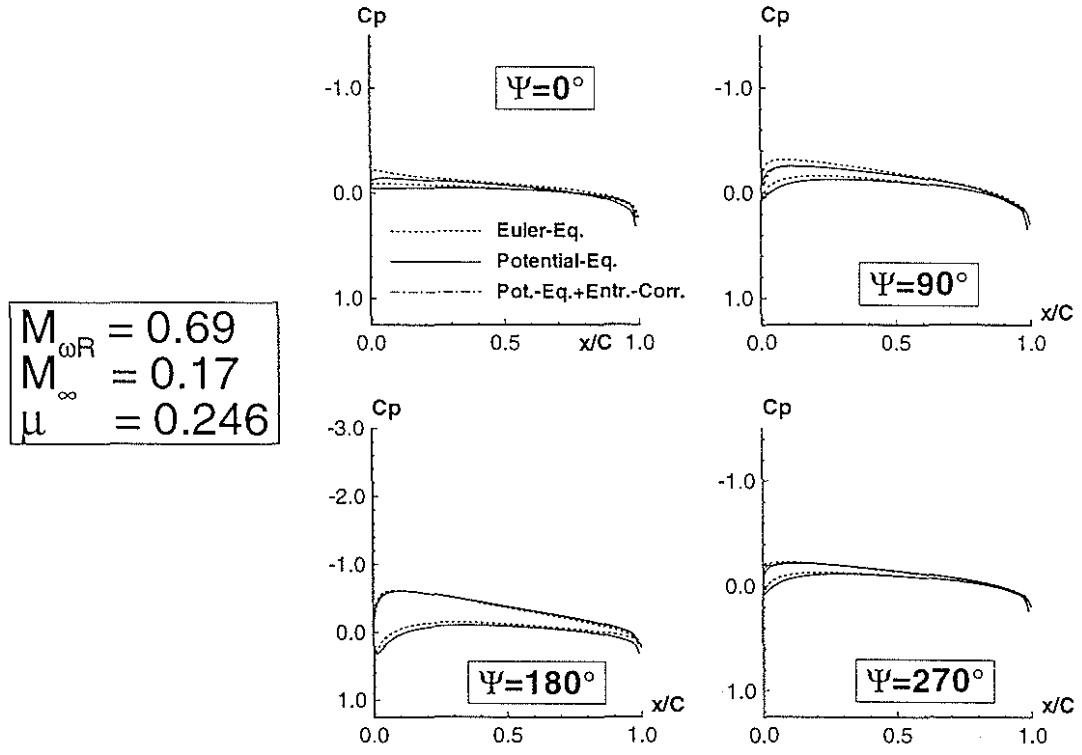

Fig. 13: Computed pressure distributions for the BERP blade in forward flight at r/R = 0.98

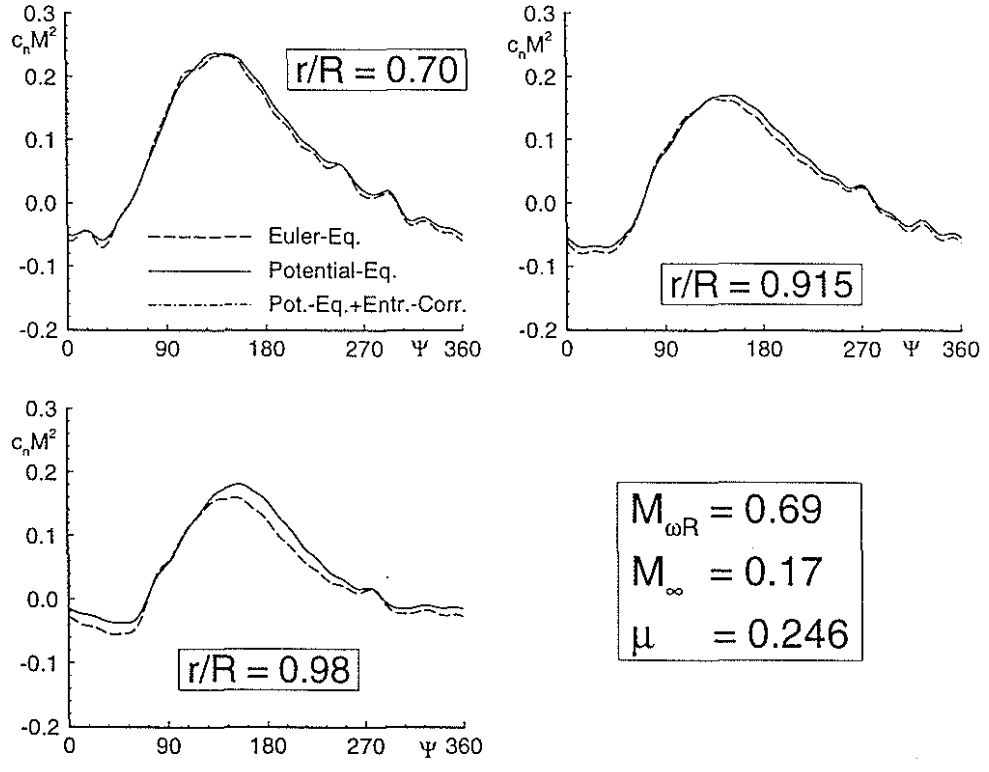

Fig. 14: Nondimensional normal forces for the BERP blade in forward flight